On the Deformation Heterogeneities Described By Crystal Plasticity

E.P. Busso
(ONERA)

E-mail: esteban.busso@onera.fr

DOI: 10.12762/2015.AL09-03

The deformation fields within grains in polycrystalline materials are generally highly heterogeneous and can be the precursors to the nucleation of micro-cracks or cavities. Such behavior is conditioned by microstructural features, such as grain structure, texture, morphology, size, etc. The understanding of such complex phenomena is crucial to enable structural integrity assessments of engineering components, since it constitutes the physical bases on which to describe the local mechanisms of deformation and failure to be incorporated into structural integrity codes. This work provides a brief overview of the different continuum mechanics approaches used to describe the deformation behavior of either single crystals or individual grains in polycrystalline metallic materials. The crucial role played by physics based local and non-local crystal plasticity approaches in the prediction of heterogeneous deformation is discussed. Representative examples are given regarding the use of dislocation mechanics-based crystal plasticity frameworks to describe localized plastic deformation behavior of FCC polycrystalline metallic materials.

Introduction

The macroscopic phenomena that control the physical and mechanical properties of materials are known to originate from the underlying microstructure. As the material characteristic length scales become smaller, its resistance to deformation becomes increasingly determined by local discontinuities, such as grain boundaries and dislocation cell walls. The interplay between grain boundary effects and slip mechanisms within a single crystal grain may result in either strength or weakness, depending on their relative sizes. Although experimental observations of plastic deformation heterogeneities are not new, the significance of these observations has not been addressed until very recently. Some experimental and numerical studies addressing the local interactions between deformation and grain boundaries have revealed how highly heterogeneous deformation states can develop locally, despite the grains being subjected to a uniformly applied macroscopic stress (e.g., [21,27,55,61,62]).

Grain interaction studies are typically concerned with the way in which uniform deformation patterns breakdown into highly localized regions of plastic deformation. Strain localization effects can differ significantly, depending on the initial texture of the material. For instance, the extent of in-grain subdivision leading to strain localization can vary significantly depending on texture ([1,44,54]). Furthermore, the initiation and subsequent development of localized deformation patterns is strongly influenced by the microstructure, particularly so in the case of somehow idealized polycrystalline systems. For example, if samples containing a small number of grains are derived from a directionally solidified material, the localization process is expected to be particularly sensitive to the relative grain sizes, arrangement and in-plane lattice misorientation between adjacent grains and within grains. The microstructural inhomogeneities resulting from these factors can easily lead to potentially 'soft' regions, which are more susceptible to extensive plastic deformation and promote strain localization. As shown in Poullier et al. [53], strain localization can be primarily driven by non-uniform lattice rotations leading to a 'geometric softening' of the crystal. The extent of the lattice rotation depends on the relative orientation between adjacent grains and on whether or not lattice misorientations are present within the grains. This is further supported by an experimental study on aluminum bicrystals [62], which showed that both low- and high-angle grain boundaries led to strain heterogeneities in the form of macroscopic shear bands. However, in this work, the extent of lattice rotation was found not to depend on the degree of misorientation between the crystals. Instead, it was found to depend on the initial pairing of orientations between adjacent crystals. In the limiting case, it is the length scales associated with the deformation patterns (e.g., the size of dislocation cells, the ladder spacing in persistent slip bands, or coarse shear band spacing) that control the material strength and ductility.

The issues discussed above, in addition to the ever increasingly powerful and sophisticated computer hardware and software available, are driving the development of novel material modeling approaches to study deformation behavior at the grain level. This work provides a brief overview of some of these approaches, based on the continuum mechanics modeling of plasticity at the grain / single crystal level. Special emphasis is placed on highlighting the crucial role that local and non-local crystal plasticity plays in developing an understanding of microstructure-related size effects on the local stress and strain fields responsible for damage initiation in polycrystalline metallic materials. Representative examples are also given about the use of such types of single crystal theories to predict size effects and localization behavior in polycrystalline FCC materials.

Single crystal plasticity

Constitutive models developed to predict the anisotropic behavior of single crystal materials generally follow either a Hill-type or a crystallographic approach. As a common feature, they treat the material as a continuum, in order to describe properly plastic or visco-plastic effects. Hill-type approaches (e.g., [56]) are based on a generalization of the Mises yield criterion proposed by Hill [40] to account for the non-smooth yield or flow potential surface required to describe the anisotropic flow stress behavior of single crystals. By modeling polycrystal structures with an appropriate crystallographic formulation based on microstructural internal state variables (e.g., dislocation densities), greater insight into the grain interaction and deformation behavior of polycrystals can be achieved. In constitutive formulations based on crystallographic slip, the macroscopic stress state is resolved onto each slip system following Schmid's law. Internal state variables are generally introduced in both formulations to represent the evolution of the microstructural state during the deformation process. Although recent developments of these two approaches have now reached an advanced stage, the major improvements made have been by crystallographic models, due to their ability to incorporate complex slip micromechanisms within their flow and evolutionary equations.

The inelastic response of metallic single crystal materials or grains is fully anisotropic and depends strongly on the shearing rate relations for the potentially active slip systems: 12 for FCC, 24 for BCC and 24 for HCP lattices. Kinetics and hardening-recovery mechanisms can also vary greatly. Typically, in dislocation density-based models, the evolution of the dislocation structure is described by processes of dislocation multiplication and annihilation, as well as by the trapping of dislocations [52,64]. Further discretization into pure edge and screw types enables their individual roles to be more clearly distinguished [8,20]. For example, edge and screw dislocations are associated with different dynamic recovery processes (i.e., climb for edges and cross-slip for screws), combining to influence the evolving dislocation structure of a deforming material. Comprehensive discussions of these issues can be found in, for instance, [17,18,35,48].

In what follows, local and non-local crystal plasticity approaches are discussed and representative applicative examples given.

Local single crystal approaches

A generic internal variable based crystallographic framework is said to be a local one when the evolution of its internal variables can be fully determined by the local conditions at the material point. The description of the kinematics of most crystal plasticity theories follows that originally proposed by Mandel [47] and by Asaro and Rice [10], which has been widely reported in the computational mechanics literature (e.g., [2,3,14,15,16,38,39]). The multiplicative decomposition of the total deformation gradient, $\mathbf{F}$ into an inelastic component $\mathbf{F}^p$, and an elastic component $\mathbf{F}^e$ is classical; i.e., under isothermal conditions,

$$\mathbf{F} = \mathbf{F}^e \, \mathbf{F}^p \tag{1}$$

Although single crystal laws can be formulated in a co-rotational frame, i.e., the stress evolution is computed on axes that rotate with the crystallographic lattice, the most widely used approach is to assume that the material's response is hyperelastic, that is, that its behavior can be derived from a potential (i.e., free energy) function. Such a potential function may be expressed in terms of the elastic Green-Lagrange tensorial strain measure,

$$\mathbf{E}^e = \frac{1}{2}\left(\mathbf{F}^{e^T}\mathbf{F}^e - I\right) \tag{2}$$

and the corresponding objective work conjugate (symmetric) stress, or second Piola-Kirchhoff stress, $\mathbf{T}$. Note that the Cauchy stress is related to $\mathbf{T}$ by

$$\sigma = det\left\{\mathbf{F}^e\right\}^{-1}\mathbf{F}^e\mathbf{T}\,\mathbf{F}^{e^T} \tag{3}$$

The hyperelastic response of the single crystal is governed by,

$$\mathbf{T} = \frac{\partial \Phi\left\{\mathbf{E}^e\right\}}{\partial \mathbf{E}^e} \tag{4}$$

where $\partial\Phi / \partial\mathbf{E}^e$ represents the Helmholtz potential energy of the lattice per unit reference volume. If small elastic stretches are assumed, then

$$\mathbf{T} \cong \boldsymbol{L} : \mathbf{E}^e \tag{5}$$

where $\boldsymbol{L}$ is the anisotropic linear elastic moduli. In rate-dependent formulations, the time rate of change of the inelastic deformation gradient, $\mathbf{F}^p$, is related to the slipping rates on each slip system as

$$\dot{\mathbf{F}}^p = \left(\sum_{\alpha=1}^{n_\alpha}\dot{\gamma}^\alpha\mathbf{P}^\alpha\right)\mathbf{F}^p \text{ with } \mathbf{P}^\alpha \equiv \mathbf{m}^\alpha \otimes \mathbf{n}^\alpha \tag{6}$$

Here, $\mathbf{m}^\alpha$ and $\mathbf{n}^\alpha$ are unit vectors defining the slip direction and the slip plane normal to the slip system.

In rate-independent formulations, in contrast, flow rules are based on the well-known Schmid law and a critical resolved shear stress, τ_c^α, whereby the rate of slip is related to the time rate of change of the resolved shear stress, $\tau^\alpha (= \mathbf{T} : \mathbf{P}^\alpha)$. Then,

$$\dot{\tau}^\alpha = \dot{\tau}_c^\alpha = \sum_{\beta=1}^{m_\alpha} h^{\alpha\beta}\dot{\gamma}^\beta \quad \text{if } \dot{\gamma}^\beta > 0 \tag{7}$$

In the above equation, $h^{\alpha\beta}$, the slip hardening matrix coefficients, incorporate latent hardening effects. Due to the severe restrictions placed on material properties, such as latent hardening, to ensure uniqueness in the slip mode (e.g., [8,17]) and the associated difficulties in its numerical implementation, the use of rate-independent formulations has been somehow restricted and much more limited than rate-dependent ones. This has been compounded by the fact that, by calibrating their strain rate sensitivity response accordingly, rate-dependent models have been successfully used in quasi-rate-independent regimes. Thus, the focus of the discussions will henceforth be on rate-dependent approaches.

The slip rate in eq. 6 can functionally be expressed as,

$$\dot{\gamma}^\alpha = \hat{\dot{\gamma}}^\alpha\left\{\tau^\alpha, \mathrm{S}_1^\alpha, \ldots, \mathrm{S}_{m_s}^\alpha, \theta\right\} \tag{8}$$

where, S_i^α (for $i = 1, \ldots, m_s$),denotes a set of internal state variables for the slip system α and θ is the absolute temperature. A useful and generic expression for the overall flow stress in the slip system can be conveniently found by inverting eq. 8. Let us, for instance, consider a case with three slip resistances $(m_3=3)$. Then,

$$\tau^{\alpha} = \pm \hat{f}_v^{\alpha} \left\{ \dot{\gamma}^{\alpha}, S_3^{\alpha}, \theta \right\} \pm c_{dis} S_1^{\alpha} \pm c_{ss} S_2^{\alpha} \qquad (9)$$

where c_{dis} and c_{ss} are scaling parameters, S_i^{α} and S_2^{α} represent additive slip resistances and S_3^{α} is a multiplicative component. Here the distinction between the additive (S_1^{α} and S_2^{α}) and the multiplicative (S_3^{α}) slip resistances is motivated by the additive nature of non-directional scalar hardening mechanisms. By expressing the flow stress as in eq. 9, the contributions from viscous effects (first term in eq. 9), and dissipative (e.g., hardening, recovery) mechanisms arising from, for instance, forest dislocation and solid solution strengthening (i.e., second and third terms), can be clearly identified. The majority of formulations rely on power law functions for eq. 8, where the resolved shear stress is normalized by a slip resistance or hardening function, which corresponds to $S_3^{\alpha} \neq 0$ and $S_1^{\alpha} = S_2^{\alpha} = 0$ in eq. 9. This introduces a coupling between the viscous term and microstructure that is inconsistent with the aforementioned additive nature of most strengthening mechanisms. Works such as those of [14,15,19] have proposed flow stress $S_1^{\alpha} \neq 0$ and $S_2^{\alpha} = S_3^{\alpha} = 0$ which allows a more physically meaningful interpretation of strengthening phenomena controlled by the dislocation structure. The particular application for FCC polycrystals to be discussed in the next section assumes that $S_1^{\alpha} \neq 0$, $S_2^{\alpha} \neq 0$ and $S_3^{\alpha} = 0$. For a more detailed discussion of these issues, see also [17].

The relation between the overall slip resistance associated with statistically stored dislocation forest-type obstacles and the individual dislocation densities is defined by,

$$S_i^{\alpha} = \lambda \mu b^{\alpha} \left\{ \sum_{\beta} h^{\alpha\beta} \rho_i^{\beta} \right\}^{1/2} \quad (\text{for } i=1, \ldots, n_s) \qquad (10)$$

Here, λ is a statistical coefficient, which accounts for the deviation from regular spatial arrangements of the dislocations, and b^{α} represents the magnitude of the Burgers vector. The corresponding total athermal slip resistance due to forest dislocations can then be expressed as

$$S_{dis}^{\alpha} = \left\{ \left(S^{\alpha}\right) + \left(S^{\alpha}\right) + \ldots + \left(S_{ns}^{\alpha}\right) \right\}^{1/} \qquad (11)$$

where $r=1$ is used when a linear sum of the slip resistances is desired, and $r=2$ is used for a mean square value.

In order to complete the set of constitutive relations, separate evolutionary equations need to be formulated for the individual dislocation densities, with dislocation multiplication and annihilation forming the bases of their evolutionary behavior [14,15].

An application of local crystal plasticity to the study of deformation heterogeneities in FCC polycrystals

In this section, the classical local single crystal framework described in the previous section will be applied to the study of intergranular cracking in an FCC Al-0.5%Mg alloy. The work to be described here is based on that by Cheong and Busso [21], who studied the effects of lattice misorientations on the development of strain heterogeneities in FCC polycrystals in a thin Al–0.5% Mg polycrystalline specimen under uniaxial tension. The geometry and test conditions of the tensile specimen were based on the experimental work of Zhang and Tong [63], using a flat specimen gauge section containing 10 mm-size grains, with one very large grain spanning almost the entire specimen width (i.e., Grain 10 in figure 1(a)).

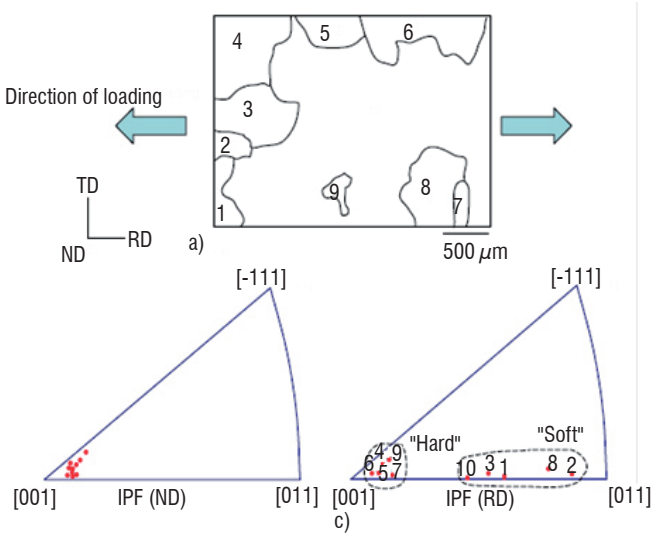

Figure 1 - (a) Initial microstructure of the Al–0.5% Mg tensile specimen (center gauge section). The inversed pole figures (IPFs) with respect to the ND direction, (b) highlights the strong ½(001) texture of the g rains with respect to the RD direction and (c) identifies the corresponding 'hard' and 'soft' orientations of the specimen's grains

Single crystal formulation

The single crystal model used for the individual grains of the FCC Al alloy was based on the original formulation proposed by [20] for Cu. The generic form of the slip rate, $\dot{\gamma}^{\alpha}$, given in eq. 8, is assumed to be dominated by the thermally activated glide of dislocations over obstacles. The slip rate is related to the resolved shear stress, τ^{α}, through the exponential function proposed by Busso [14] (see also [15,16]),

$$\dot{\gamma}^{\alpha} = \dot{\gamma}_o exp\left[-\frac{F_o}{k\theta} \left\{ 1 - \left\langle \frac{\left|\tau^{\alpha}\right| - S^{\alpha}\mu/\mu_o}{\hat{\tau}} \right\rangle^{p} \right\}^{q} \right] sign(\tau^{\alpha}) \qquad (12)$$

which accounts for the absolute temperature (θ, K) and the stress dependence of the activation energy. In eq. 12, F_0 represents the Helmholtz free energy of activation at $0\,K$, k is the Boltzmann constant, $\dot{\gamma}_o^{\alpha}$ is a reference slip rate and is the maximum glide resistance at which dislocations can be mobilized without thermal activation. Furthermore, μ and μ_0 are the shear moduli at θ and $0\,K$, respectively. The exponents p and q describe the shape of the energy barrier vs. the stress profile associated with interactions between dislocations and obstacles.

The athermal slip resistance, S^{α}, is expressed as

$$S^{\alpha} = \lambda \mu b^{\alpha} \sqrt{\left(\sum_{\beta=1}^{N} h^{\alpha\beta} \rho_T^{\beta} \right)} \qquad (13)$$

where the overall dislocation density for a given slip system β, ρ_s^{β} is obtained from a discretization of the dislocation structure into pure edge and pure screw types, of densities ρ_e^{β} and ρ_s^{β}, respectively. Thus,

$$\rho_T^{\beta} = \rho_e^{\beta} + \rho_s^{\beta} \qquad (14)$$

The evolutionary equations of the individual dislocation densities account for the competing dislocation storage-dynamic recovery processes and are expressed as [19,21],

$$\dot{\rho}_e^{\alpha} = \frac{C_e}{b^{\alpha}}\left[K_e \sqrt{\sum_{\beta=1}^{N} \rho_T^{\beta}} - 2d_e \rho_e^{\alpha} \right] \left| \dot{\gamma}^{\alpha} \right| \quad (15)$$

and

$$\dot{\rho}_s^{\alpha} = \frac{C_s}{b^{\alpha}}\left[K_s \sqrt{\sum_{\beta=1}^{N} \rho_T^{\beta}} - \rho_s^{\alpha} \left(\pi d_s^2 K_s \sqrt{\sum_{\beta=1}^{N} \rho_T^{\beta}} + 2d_s \right) \right] \left| \dot{\gamma}^{\alpha} \right| \quad (16)$$

Here, the parameters C_e and C_s describe the relative contributions to the overall slip from edge and screw dislocations, while K_e and K_S are mobility constants associated with their respective mean free paths. Recovery processes are associated with the parameters d_e and d_s, which represent critical annihilation distances between dislocations of opposite Burgers vectors for both edge and screw types.

The calibration of the model's parameters was inspired by those reported for pure aluminum by [21]. In order to account for the increase in yield strength from solid-solution strengthening, the initial value of the slip resistance, S^{α}, was adjusted to provide a suitable yield strength value associated with the Al–0.5% Mg alloy. For details about the implicit numerical implementation of the above constitutive theory into the finite element method, refer to ref. [16].

Predicted deformation patterns and plastic strain distribution

Two cases with slightly different microstructural textures were considered. In Case 1, the lattice orientation of each grain was assumed to be uniform. In contrast, Case 2 assumed that within each grain, there exists a random distribution of misorientations ranging from 0° to 6°, which is typical of those found in polycrystalline aggregates. The measured and predicted deformed shape of the tensile specimens after 12% true strain is shown in figure 2. In figure 2(a), the middle section shows the distinct formation of a macroscopic shear band spanning the entire specimen width for Case 1. This is less apparent in figure 2(b) for Case 2, where deformation appears more homogeneous. Figure 2(c) presents the experimentally measured contour plots of the accumulated plastic axial strain, which reveal that the predicted local strain measurements are in agreement with those in the actual deformed specimen. In both cases, the central region of the shear bands is tilted approximately 25° from the transverse direction. However, the predicted magnitude and distribution of the accumulated plastic axial for Case 2 are closer to those in the actual specimen than Case 1. Figure 3 shows the corresponding plastic strain distributions across the specimens for Case 2 after 5 and 1% true strain. Here, the plotted strain quantity is simply defined as $\left(\varepsilon_{11}^{p} = F_{11}^{p} - 1\right)$, where the subscript '11' represents the axial component of the plastic deformation gradient, which coincides with the rolling direction (RD). Qualitatively, both Cases 1 and 2 predict the distinct formation of an inclined macroscopic shear band, which extends across the width of the specimen, in agreement with the local strain measurements in the actual deformed specimen. In both cases, the central region of the shear bands are tilted approximately 25° anti-clockwise from the transverse direction, similar to the measurements on the actual deformed specimen. However, they differ from each other as well as from the actual specimen in terms of the magnitude and distribution of the accumulated plastic axial strain. In Case 1, a rather sharp and highly localized shear band is predicted in the middle of the gauge section, with local strains more than seven times greater than the macroscopically applied uniaxial strain. In the surrounding regions, the plastic strain distribution is uniform and significantly lower, indicating that the bulk of the plastic deformation in the specimen is now accommodated within the band. In contrast, the Case 2 assumption leads to the development of a less intense shear band in the same region, which agrees more closely with the experimental evidence.

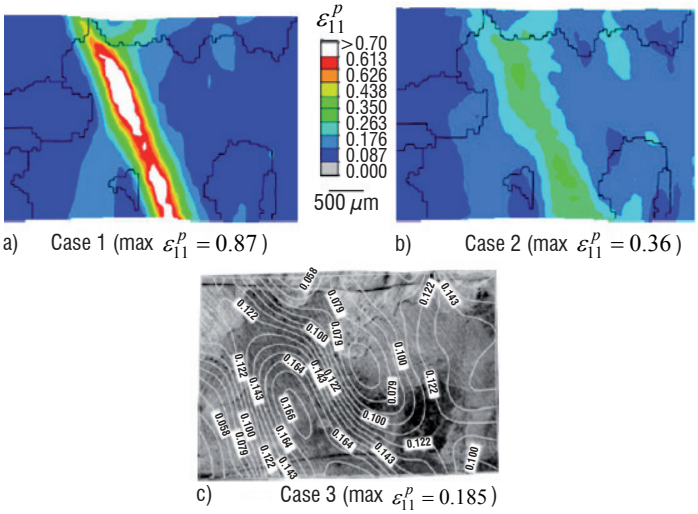

Figure 2 - Comparison between the predicted and experimentally measured distributions of accumulated plastic axial strain ε_{11}^{p} in the polycrystal for (a) Case 1 (uniform lattice orientations within each grain), (b) Case 2 (intragranular lattice misorientations) and (c) the actual tensile specimen after 12% true strain [63].

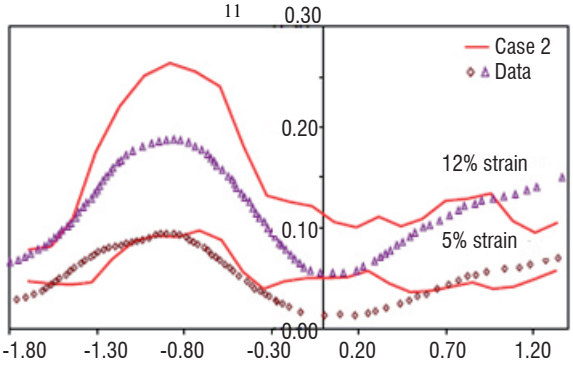

Figure 3 - Comparison between the accumulated plastic axial strain profiles along the specimen center line at 5% and 12% true strains. The open symbols are experimentally measured values [63], and the solid lines are the Case 2 predictions.

These results are consistent with a recent study on a Cu tensile specimen [19], which showed that the presence of intragranular misorientations serves to redistribute plastic strain and reduces the extent of the strain localization region, resulting in a higher average deformation within each grain.

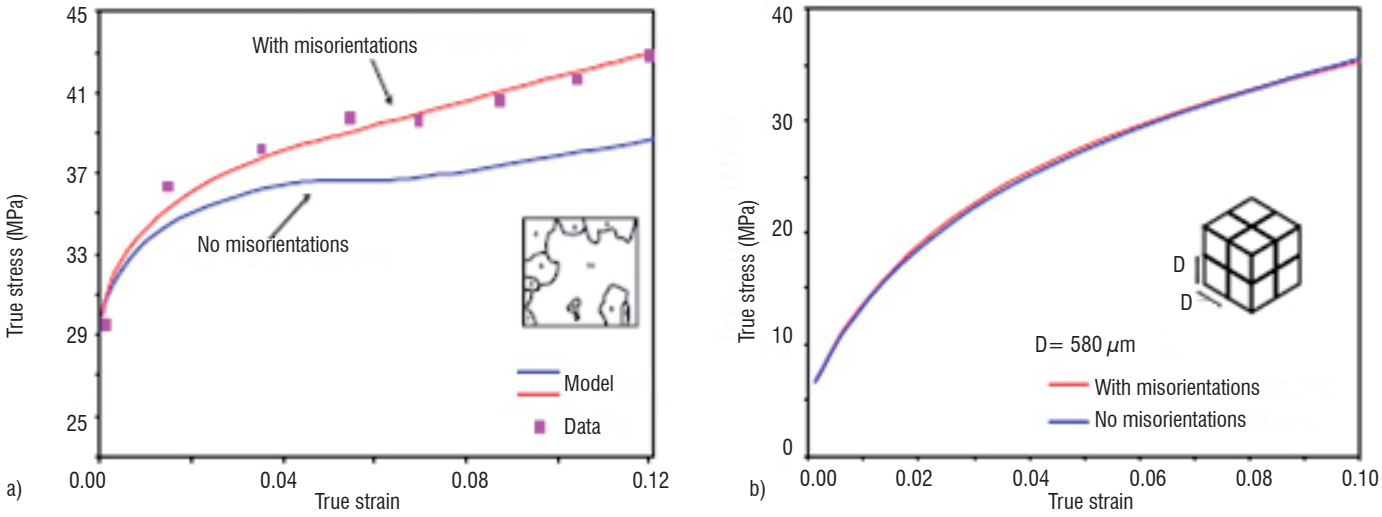

Figure 4 - The effect of intragranular misorientations on (a) thin and (b) bulk polycrystals. In (a), the experimental true stress–strain data from [63] is included to highlight the higher work hardening rate associated with the presence of intragranular lattice misorientations.

Effect of lattice misorientations on macroscopic stress-strain behavior

The difference in the macroscopic behavior of the polycrystal specimen for the case with and without intragranular lattice misorientations is shown in figure 4. The figure reveals that a higher work-hardening rate is predicted when lattice misorientations within the grains are accounted for, in agreement with the measured stress–strain response. The sensitivity of the macroscopic response to the inclusion of intragranular misorientations stems from the small number of grains in the microstructure. When high-angle boundaries are few and far between, deformation behavior is primarily dictated by the significantly larger number of low angle grain boundaries. This suggests that the mechanical behavior of such quasi two-dimensional polycrystals is more sensitive to grain substructural changes than bulk polycrystalline specimens. To confirm this, a simple study was carried out on bulk polycrystalline Al represented by an 8-grain representative volume element (RVE) with imposed periodic boundary conditions. The predicted macroscopic responses of the polycrystalline RVE up to 10% tensile strain are given in figure 4(b). It can be seen that, when compared with the thin polycrystal response of figure 4(a), the influence of intragranular misorientations in the polycrystal aggregate is negligible.

Additional results reported by [21] showed that a change of one most dominant grain in the polycrystal from a 'soft' to 'hard' initial orientation in relation to the direction of applied loading, resulted in a significant change in deformation behavior of the specimen, leading in turn to a stronger macroscopic polycrystalline response and a change in location of the localized deformation region. It could then be implied that shear bands can be expected to typically initiate in, and propagate through, grains with 'soft' orientations, thus avoiding grains with 'hard' orientations. Thus, in such thin polycrystalline specimens, a shear band need not necessarily follow a continuous straight line path but would take a path dependent upon the crystallographic orientation of the grains.

In summary, the results reported in this section have shown that a dislocation density based crystal plasticity model is capable of capturing the development of a macroscopic shear band identified experimentally. It has also been found that intragranular misorientations exert a strong influence on the deformation behavior of such polycrystals, where the total number of grains is small. However, their influence diminishes when the number of grains increases and is effectively negligible when bulk polycrystals are considered. At the local level, the prediction of the accumulated plastic axial strain distribution was found to be consistent with the experimental trend.

Non-local single crystal approaches

Most continuum approaches and formulations dealing with experimentally observed size effects in metallic materials are based on strain-gradient concepts and are known as non-local theories since the material behavior at a given material point depends not only on the local state but also on the deformation of neighboring regions. Gradient-dependent behavior becomes important once the length scale associated with the local deformation gradients becomes sufficiently large when compared with the controlling microstructural feature (e.g., average grain size in polycrys-tal materials). In such cases, the conventional crystallographic framework discussed in the previous sections will be unable to predict properly the evolution of the local material flow stress. Examples of such phenomena include particle size effects on composite behavior (e.g., [50]), precipitate size in two-phase single crystal materials [16,49], increase in measured micro-hardness with decreasing indentor size (e.g., [60]), and decreasing film thickness (e.g., [41]), amongst others.

The modeling of size effects in crystalline solids has been addressed by adding strain gradient variables into the constitutive framework, either in an explicit way in the flow rule (e.g., [6]); or in the evolutionary equations of the internal slip system variables (e.g., [4,12,16]), or by means of additional degrees of freedom associated with higher order boundary and interface conditions (e.g., [57]). The resulting strain gradient components are related to the dislocation density tensor introduced by Nye [51]. For the later, the dislocation density tensor is computed from the rotational part of the gradient of plastic deformation, so the resulting partial differential equations to be solved are generally of higher order than those used in classical mechanics. In what follows, examples of the last two types of formulations will be discussed.

Non-local models based on internal strain gradient variables

The more physically intuitive continuum approaches to describe strain gradient effects are constitutive theories (e.g., [4,9,12,16,20,29])

which rely on internal state variables to describe the evolution of the obstacle or dislocation network within the material and generally introduce the strain gradient effects directly in the evolutionary laws of the slip system internal variables without the need for higher order stresses. This requires that the overall slip resistance arising from the dislocation network, S^{α}_{dis} (see eq. 11), incorporates contributions from both statistically stored (SS) and geometrically necessary (GN) forest dislocations.

The general form for the functional dependency of the slip system internal variable evolutionary laws, extended to include the additional dependency on the GNDs and the gradient of the slip rates, $\nabla\dot{\gamma}^{\alpha}$, is

$$\begin{aligned}
\dot{\rho}^{\alpha}_{1} &= \hat{\dot{\rho}}^{\alpha}_{1}\left\{\dot{\gamma}^{\alpha},\rho^{\alpha}_{1},\ldots,\rho^{\alpha}_{n_s+n_G},\theta\right\}\\
&\vdots\\
\dot{\rho}^{\alpha}_{n_s} &= \hat{\dot{\rho}}^{\alpha}_{n_s}\left\{\dot{\gamma}^{\alpha},\rho^{\alpha}_{1},\ldots,\rho^{\alpha}_{n_s+n_G},\theta\right\}\\
\dot{\rho}^{\alpha}_{n_s+1} &= \hat{\dot{\rho}}^{\alpha}_{n_s+1}\left\{\dot{\gamma}^{\alpha},\rho^{\alpha}_{n_s+1},\ldots,\rho^{\alpha}_{n_s+n_G},\nabla\dot{\gamma}^{\alpha},\theta\right\}\\
&\vdots\\
\dot{\rho}^{\alpha}_{n_s+n_G} &= \hat{\dot{\rho}}^{\alpha}_{n_s+n_G}\left\{\dot{\gamma}^{\alpha},\rho^{\alpha}_{n_s+1},\ldots,\rho^{\alpha}_{n_s+n_G},\nabla\dot{\gamma}^{\alpha},\theta\right\}
\end{aligned} \tag{17}$$

where n_s and n_G denote the number of SSD and GND types, respectively. Consider the particular case where $n_s = 2$ and $n_G = 3$. Then, the total dislocation density on an arbitrary slip system becomes,

$$\rho^{\alpha}_{T} = \left(\rho^{\alpha}_{e} + \rho^{\alpha}_{s}\right) + \left(\rho^{\alpha}_{Gs} + \rho^{\alpha}_{Get} + \rho^{\alpha}_{Gen}\right) \tag{18}$$

where $\left(\rho^{\alpha}_{e},\rho^{\alpha}_{s}\right)$ are the SS densities and $\left(\rho^{\alpha}_{Gs},\rho^{\alpha}_{Get},\rho^{\alpha}_{Gen}\right)$ the GND densities, which have in addi-tion, been discretized into pure edge and screw components. Note that the inclusion of the out-of-plane edge dislocation density component accounts for dislocation segments, which may either have a non-planar orientation or an out-of-plane kink component with respect to the slip plane.

The evolution of the GNDs can be expressed in terms of a mathematically equivalent GND density vector, $\dot{\boldsymbol{\rho}}^{\alpha}_{G}$, defined so that its projection into the local $(\mathbf{m}^{\alpha},\mathbf{n}^{\alpha},\mathbf{t}^{\alpha})$ orthogonal reference system is as follows [16,19],

$$\dot{\boldsymbol{\rho}}^{\alpha}_{G} = \dot{\rho}^{\alpha}_{Gs}\mathbf{m}^{\alpha} + \dot{\rho}^{\alpha}_{Get}\mathbf{t}^{\alpha} + \dot{\rho}^{\alpha}_{Gen}\mathbf{n}^{\alpha} \tag{19}$$

Subsequently, the evolutionary law for each set of GNDs is determined from Nye's dislocation density tensor, $\boldsymbol{\Gamma}$ [51], in terms of the spatial gradient of the slip rate,

$$\dot{\boldsymbol{\Gamma}} = \operatorname{curl}\left(\dot{\gamma}^{\alpha}\mathbf{n}^{\alpha}\mathbf{F}^{p}\right) = b^{\alpha}\left(\dot{\rho}^{\alpha}_{Gs}\mathbf{m}^{\alpha} + \dot{\rho}^{\alpha}_{Get}\mathbf{t}^{\alpha} + \dot{\rho}^{\alpha}_{Gen}\mathbf{n}^{\alpha}\right) \tag{20}$$

Under small strains and rotations, eq. 20 simplifies to

$$\begin{aligned}
\dot{\rho}^{\alpha}_{Gs} &= \frac{1}{b^{\alpha}}\nabla\dot{\gamma}^{\alpha}\cdot\mathbf{t}^{\alpha}\\
\dot{\rho}^{\alpha}_{Get} &= \frac{1}{b^{\alpha}}\nabla\dot{\gamma}^{\alpha}\cdot\mathbf{m}^{\alpha}\\
\dot{\rho}^{\alpha}_{Gen} &= 0
\end{aligned} \tag{21}$$

The slip resistance contributions from the SSDs and GNDs can then be determined from eq. 13, using the definition of the overall dislocation density given by eq. 18. This class of theories has been shown to be capable of providing a good physical insight into the effects of microstructure on the observed macroscopic phenomena, including rate-independent plastic deformation and visco-plasticity in both single crystal and polycrystalline materials. An additional attractive feature of these theories is that they are relatively easy to implement numerically and do not require higher order stresses and additional boundary conditions or independent degrees of freedom. However, some of their limitations are that (i) they are unable to describe problems that may require non-standard boundary conditions, such as the boundary layer problem modeled in [57] and that (ii) they may exhibit a mesh sensitivity in cases where there is a predominance of geometrically necessary dislocations relative to statistically stored dislocations [20].

An application to the prediction of deformation in a channel die compression test

In this section, a study by Abrivard [1] about the deformation heterogeneities and grain fragmentation induced by the deformation of pure Al in a channel using the non-local single crystal formulation described in the previous section [19] is summarized. Such type of test is generally used to simulate cold rolling of aluminum, see figure 5. Here, the die imposes a nominally plane strain deformation gradient on the metal similar to that experienced by the aluminum passing through a rolling mill. Furthermore, the channel walls suppress the lateral material flow and induce heterogeneous lateral stresses in the deforming material. Details about the experiment can be found in [1].

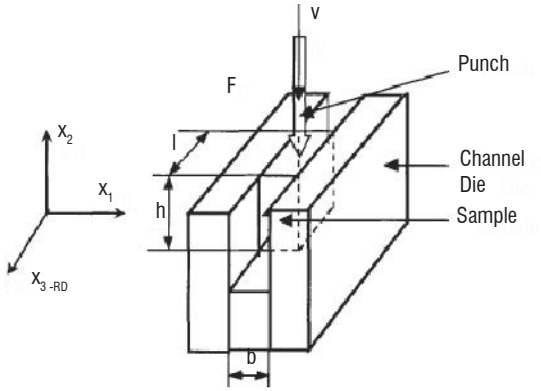

Figure 5 - Channel die compression test layout

The investigation of in-grain subdivision and inter-grain misorientations in a polycrystalline aggregate requires that the local density of geometrically necessary boundaries (GNB) be accounted for. The polycrystal material used in the channel die test model was assumed to be composed of a random distribution of grain orientations, with the initial texture as shown in figure 5(a). Here, polycrystalline aggregates containing either 20 or 40 grains with an average 100 μm size were considered in this study. Boundary conditions were applied such that a sample height reduction by compression along the x_2 axis (ND) of up to 60% was achieved. The numerical results of the deformed aggregate under plane strain compression are discussed next.

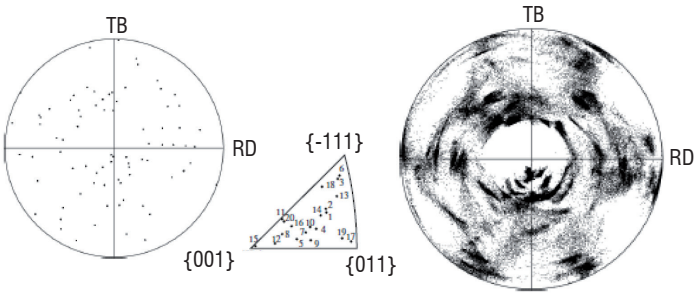

Figure 6 - (a) {111} pole and {001} inverse pole figures showing the polycrystalline aggregate initial grain orientations and (b) {111} pole figure after 60% height reduction

During deformation, grains rotate and break into subgrains with different slip system activity. As GNDs build-ups are associated with gradients of slip-rate, the number of GNDs increases signifi-cantly inside the grains. Contrary to the second gradient and Cosserat theories, no term in the free energy penalizes their development. Therefore, the determination of slip-rate gradients with the non-local theory used here could be sensitive to the mesh size. In order to attenuate this problem when solving the evolutionary laws for the GNDs densities, a quantity defined as $A = \gamma^{\alpha} n^{\alpha} F^{p}$ is calculated at the Gauss point of interest, as well as at neighboring ones found within a critical distance linked to the GNDs spread from the grain boundary [45]. Here, that distance was assumed to be given by the mean grain size. The field of the quantity A is then used to compute curl(A) at that point through a linear interpolation and the latter subsequently used to evaluate the evolution of the individual GND densities as per eq. 19 and 21.

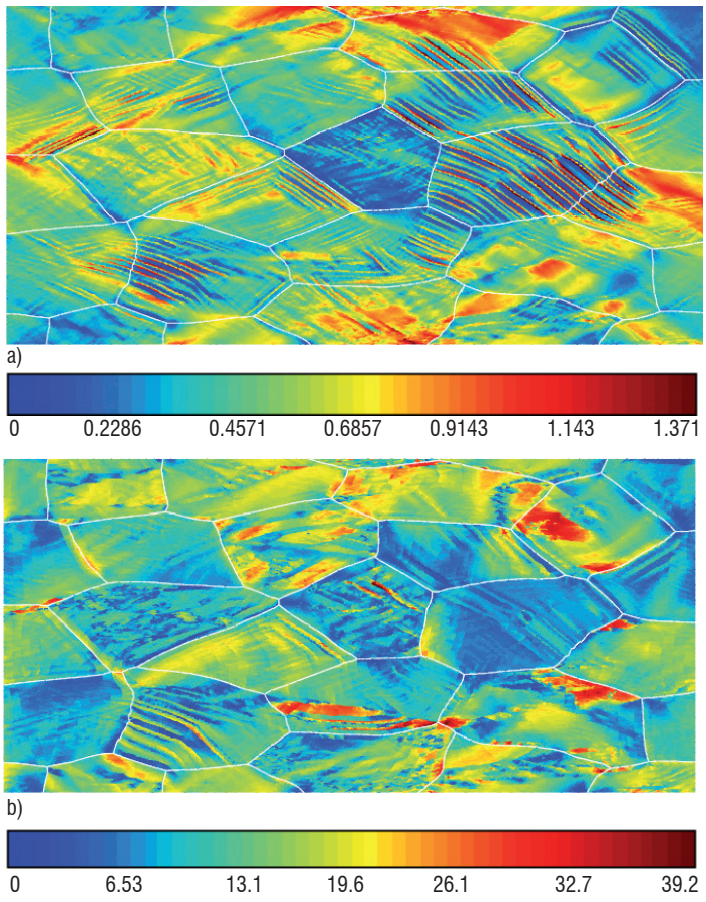

Figure 7 - (a) Accumulated inelastic strain contours
(b) Corresponding lattice rotations distribution after 30% height reduction

Figure 7 shows the predicted (a) accumulative inelastic strain contours and (b) the corresponding accumulated lattice rotations up to 30% compression. It can be seen that the predictions reveal deformation heterogeneities: grains break up into macroscopic deformation bands aligned along the 40° shear directions (towards the rolling direction, x3-axis in figure 5). This deformation process leads finally to the formation of a micro-band structure as straight dense dislocation walls run parallel to each other along preferred directions, leading to the multiplication of GNDs inside the grains. Since GNDs accommodate lattice incompatibilities in regions where the deformation is inhomogeneous, their local density can be related to the local lattice curvature described by the predicted accumulated lattice rotations in figure 7(b). It can also be seen that rotation bands are found in the same grains as those that have developed deformation bands.

Substructure description

During the deformation of high stacking fault energy of pure metals such as Al and its alloys, grains generally develop substructures, which may be classified into two different types: incidental dislocation boundaries (IDB) and geometrically necessary boundaries (GNB), see figure 9. These two types of boundary form differently: IDBs do so by the random trappings of glide dislocations, while GNBs form to accommodate the increasing subdivision of grains during confined deformation into smaller regions with rather different lattice orientations. IDBs are made up mostly of statistically stored dislocations, which do not contribute significantly to a net lattice rotation, whereas GNBs are composed of excess dislocations, which are geometrically necessary and contribute to the net lattice rotation. The size of either such regions or dislocation cells depends on the deformation level, the grain orientation and the loading path. At small strains, GNBs form elongated cell blocks surrounding regions that are almost dislocation free. At larger levels of strain, the average GNB misorientation increases and their spacing decreases.

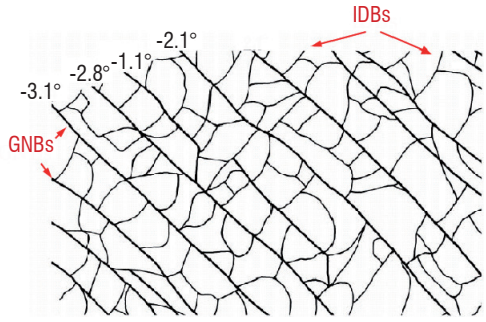

Figure 9 - Schematic representation of a grain subdivided into regions delimited by geometrically necessary boundaries (GNBs) and intense dislocation boundaries (IDBs) [46]

Under large deformations, IDs can be further sub-divided into dislocation cells whose sizes are generally reported to be less than 3 μm for pure aluminum. Thus, since the smallest finite ele-ment size used in the simulations is of the order of 4 μm, the model resolution is insufficient to describe the formation of dislocation cells explicitly. Nevertheless, it will be shown here that it is possible to predict the fragmentation of the grain in a realistic way. An example is shown in the inverse pole figure of figure 10 of the polycrystal aggregate after a

40% height reduction. The grain fragmentation is underlined through the relative misorientation between neighboring points, which have been superimposed onto the inverse pole figure of the aggregate. Here, black points or lines represent material points with neighboring sites having a relative lattice misorientation of at least 15°, blue points those with misorientations of between 5° and 15°, and gray points with those between 1° and 5°. From such type of information, as well as the local dislocation densities, it is possible to estimate the cell size statistically. It should be noted that TEM observations have shown that cell shape can vary with the grain orientation, here such dependency was not considered for simplicity.

In order to determine the cell size from the spacing between intense dislocation bands (IDBs) formed by the random trappings of glide dislocations, a relation was used by [1] which relies on statistically stored dislocation densities such that,

$$d_{IDB} = \frac{K_{IDB}}{\sqrt{\rho_{SSD}}} \tag{22}$$

where K_{IBD} is a parameter to be calibrated from experimental data. From the IDB measurements on pure Al reported by [42], $K_{IBD} = 8.5$. The resulting predicted IDB spacings calculated at each integration point of the FE model are plotted in figure 11(a) as a cloud of gray points, with their average predictions given by the red line. It can be seen that a broad range of IDBs spacing is found for the same level of equivalent strain and that the associated average predicted curve exhibits the same trend as the experimental data reported by [42].

Since geometrically necessary boundaries (GNBs) are also generated between regions to accommodate the lattice rotation differentials, only geometrically necessary dislocations are taken into account in a relation of the same type as that of eq. (22),

$$d_{GNB} = \frac{K_{GNB}}{\sqrt{\rho_{GND}}} \tag{23}$$

where $K_{IBD} = 8.5$. In figure 11(b), the predicted GNB spacing vs. the equivalent strain is in good agreement for strains greater than 25 %. Experimental data from [42] showed that GNB spacing ranges from 3 μm for strains of approximately 12% to 0.3 μm for 100% strain, just in the limits of the FE model resolution. Thus these results should be perceived as a statistical average.

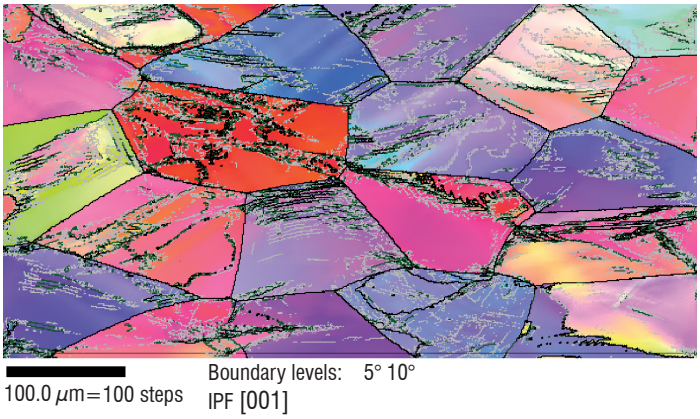

Figure 10 - [001] inverse pole figure of the polycrystalline aggregate after 40% height reduction

The above numerical predictions of the confined deformation behavior of an aluminum aggregate using a non-local dislocation density based crystal plasticity framework have shown to capture the main characteristics of the deformation heterogeneities seen experimentally, such as grain fragmentations and the development of deformation bands. Such realistic simulations are obtained despite the inherent spatial resolution limitations of the finite element model in the channel die compression test.

Non-local models based on the mechanics of generalized continua

Approaches based on the so-called mechanics of generalized continua incorporate, as a common feature, extra-hardening effects associated with the dislocation density tensor. Generalized crystal plasticity models developed in the past forty years can be classified into two main groups. In the first one, strain gradient plasticity models involve either the rotational part of the plastic distortion (i.e., the plastic rotation), its full gradient, or just the gradient of its symmetric part [32,36,37,58]. The second group involves generalized continuum theories with additional degrees of freedom accounting for either the rotation or the full deformation of a triad of crystal directors and the effect of their gradients on hardening, such as Cosserat-type models [22,33], and those based on the micromorphic theory [11,23,24,25,31].

Most of these theories have been shown to capture size effects, at least in a qualitative way. However, a clear demonstration that they can reproduce the scaling laws expected in precipitate hardening or grain

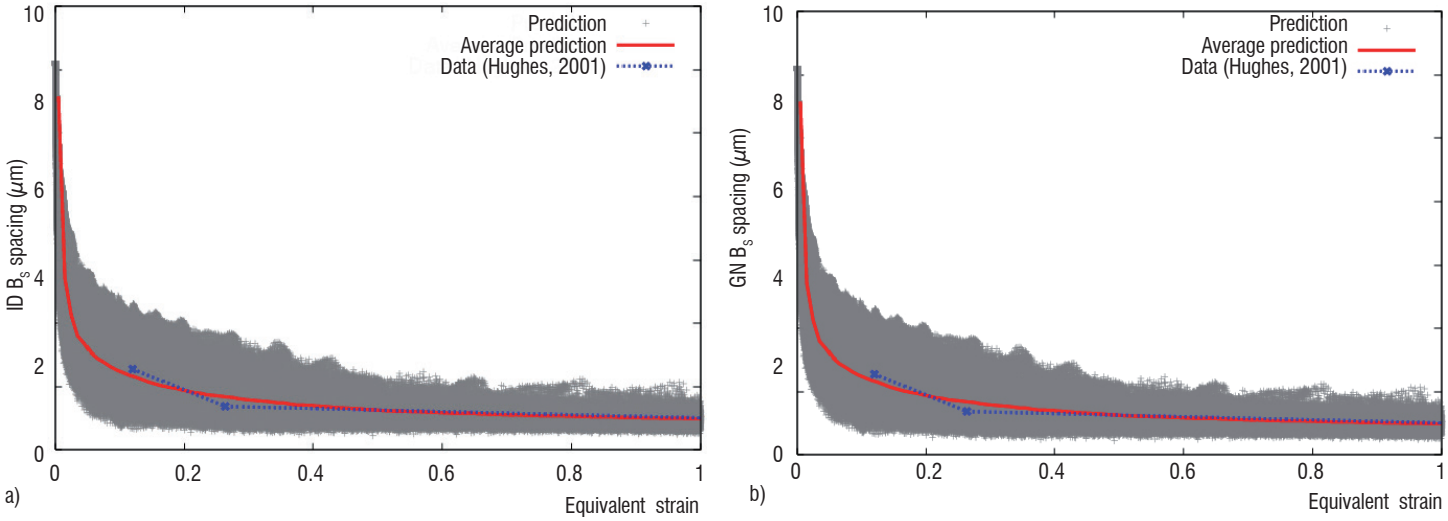

Figure 11 - Comparison between the predicted and experimental (a) IDB and (b) GNB spacing

size effect has not been fully provided yet. The additional hardening effects inherent in generalized continuum crystal plasticity models can be summarized by the main fea-tures identified in figure 12. Here, the effect of the dominant microstructural length scale, l, such as grain or precipitate size, on the material flow stress, is shown schematically in a log–log diagram. The curve can be characterized by three main features: the stress range, $\Delta\Sigma$, the characteristic length, l_c, and the slope of the intermediate region, defined by a scaling law of the form, $\Sigma \propto l^n$ at $l=l_c$. Here, $\Delta\Sigma$ corresponds to the maximum increase in strength due to size effects relative to the size-independent level. Figure 12 shows that when the characteristic size of the microstructure decreases, the material strengthens. For large values of l, the asymptotic behavior corresponds to the size-independent response of conventional crystal plasticity models reviewed in a previous section. In contrast, for small values of l, a bounded or unbounded asymptotic behavior can be obtained, depending on the type of model considered. Cosserat-type crystal plasticity models (e.g., [33]), for instance, predict an asymptotically saturated over-stress $\Delta\Sigma$ as in figure 12. In the intermediate region, when l is close to the characteristic length, l_c, the size-dependent response is characterized by the scaling law, $\Sigma \propto l^n$. The parameters $\Delta\Sigma$, l_c and n can be derived explicitly for the different classes of generalized material models described above. However, an analytic description of the size-dependent behavior of materials is possible only for some specially simplified geometrical situations. Examples are the shearing of a single crystal layer under single (or double) slip for strain gradient plasticity models considered in [13,23,24,25,43,57], and the single slip in a two-phase laminate microstructure by [34].

When crystal plasticity is considered under small strain assumptions, the gradient of the velocity field can be decomposed into the elastic and plastic distortion rates:

$$\dot{\mathbf{H}} = \dot{\mathbf{u}} \otimes \nabla = \dot{\mathbf{H}}^{\mathrm{e}} + \dot{\mathbf{H}}^{\mathrm{p}} \tag{24}$$

where

$$\dot{\mathbf{H}}^{\mathrm{p}} = \sum_{\alpha} \dot{\gamma}^{\alpha} \mathbf{P}^{\alpha} \tag{25}$$

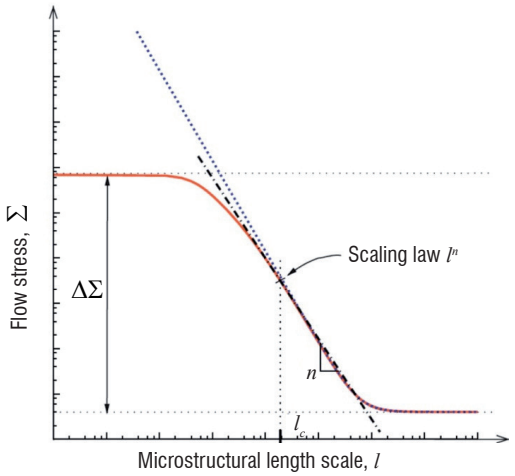

Figure 12 - Effect of the dominant microstructural length scale, l, on the material flow stress, Σ, predicted by various types of models, such as those exhibiting two asymptotic regimes (solid line) and others that exhibited an unbounded flow stress for small length scales (dotted line). Also included is the scaling law in the transition domain (dot-dashed line) [43]

with, u, the displacement field, α the number of slip systems, $\dot{\gamma}^{\alpha}$ the slip rate for the slip system α, and $\mathbf{P}^{\alpha}$ as defined in eq. 6. The elastic distortion tensor, $\mathbf{H}^e$, which represents the stretch and rotation of the lattice, links the compatible total deformation, $\mathbf{H}$, with the incompatible plastic deformation, $\mathbf{H}^p$, which describes the local lattice deformation due to the flow of dislocations. On account of eq. 24 and since applying the curl operator to the compatible field represented by $\mathbf{H}$ is equal to zero, it follows that

$$\operatorname{curl} \dot{\mathbf{H}} = 0 = \operatorname{curl} \dot{\mathbf{H}}^{\mathrm{e}} + \operatorname{curl} \dot{\mathbf{H}}^{\mathrm{p}} \tag{26}$$

The incompatibility of the plastic distortion is characterized by its curl part, also known as the dislocation density tensor or Nye's tensor [4,51,58], defined as

$$\boldsymbol{\Gamma} = -\operatorname{curl} \mathbf{H}^{\mathrm{p}} = \operatorname{curl} \mathbf{H}^{\mathrm{e}} \tag{27}$$

The tensors $\mathbf{H}$, $\mathbf{H}^e$, and $\mathbf{H}^p$, are generally non-symmetric, thus they can be decomposed into their symmetric and skew-symmetric parts:

$$\mathbf{H} = \mathbf{E} + \mathbf{W}, \mathbf{H}^e = \mathbf{E}^e + \mathbf{W}^e, \mathbf{H}^p = \mathbf{E}^p + \mathbf{W}^p \tag{28}$$

Combining eqs. 26 and 28 leaves

$$0 = \operatorname{curl} \mathbf{E}^e + \operatorname{curl} \mathbf{W}^e + \operatorname{curl} \mathbf{H}^p \tag{29}$$

Neglecting the curl part of the elastic strain, $\mathbf{E}^e$, leads to the following approximation of the dislocation density tensor derived by Nye:

$$\boldsymbol{\Gamma} = \operatorname{curl} \mathbf{H}^e = \operatorname{curl} \mathbf{E}^e + \operatorname{curl} \mathbf{W}^e \approx \operatorname{curl} \mathbf{W}^e \tag{30}$$

Thus, Nye's formula sets a linear relationship between the dislocation density tensor and the lattice curvature defined by $\mathbf{W}^e$. The Cosserat crystal plasticity theory accounts for the effect of lattice curvature on the crystal hardening behavior by incorporating the three additional independent degrees of freedom associated with the components of the lattice rotation, $\mathbf{W}^e$. In contrast, theories such as those proposed by [36] and [59], for example, include the full curl of the plastic distortion, $\mathbf{H}^p$, as an independent internal variable of the constitutive model. This requires, in general, nine additional degrees of freedom associated with the generally non-symmetric plastic distortion tensor, $\mathbf{H}^p$. This sub-class of models is sometimes referred to as 'curl $\mathbf{H}^p$'- type [23]. A consequence of neglecting the curl of the elastic strain tensor in Cosserat-type models is that Cosserat effects can arise, even in the elastic regime, as soon as a gradient of ''elastic'' rotation exists (i.e., $\operatorname{curl} \mathbf{W}^e \neq 0$). This implies that as soon as the $\operatorname{curl} \mathbf{E}^e \neq 0$, the $\operatorname{curl} \mathbf{W}^e \neq 0$. In contrast, in the curl -type theories, strain gradient effects can only arise when plastic deformation has developed. As has been shown in [23], this can lead to discontinuities in the generalized tractions at the interface between elastic and plastic regions. For the $\operatorname{curl} \mathbf{H}^p$-type models, it is necessary to identify numerically higher order boundary conditions at the elasto-plastic boundaries, which poses difficulties in the numerical implementation of this type of formulations, as discussed in [23].

To overcome the limitations of both the Cosserat and $\operatorname{curl} \mathbf{H}^p$-type theories, a new regularization method has recently been proposed by Cordero et al. [23] (see also [24,25]). Their model, which they have called *microcurl*, falls into the class of generalized continua with additional degrees of freedom. Here, the effect of the dislocation density

tensor is introduced into the classical crystal plasticity framework by means of the micromorphic theory of single crystals. It relies on the introduction of an additional plastic micro-deformation variable, $\boldsymbol{\chi}^p$, a second-rank generally non-symmetric tensor. It is distinct from the plastic distortion tensor $\mathbf{H}^p$, which is still treated as an internal variable of the problem, in the same way as in $\mathrm{curl}\,\mathbf{H}^p$-type theories. For the general three dimension case, the nine components of $\boldsymbol{\chi}^p$ are introduced as independent degrees of freedom. For full details about the microcurl theory, the reader is referred to [18,23,24,25].

An application of the microcurl model to study the deformation behavior of a polycrystalline aggregate

The microcurl model was applied to study the global and local responses of two-dimensional polycrystalline aggregates with grain sizes ranging from 1 to 200 microns (For full details about this work, refer to [25]). A typical result from this work about the effect of grain size on the way plastic deformations in polycrystals evolve is shown in figure 13 for a 52-grain aggregate. These contour plots show the field of equivalent plastic deformation, $\tilde{\varepsilon}^p$, defined as the time-integrated value of

$$\dot{\tilde{\varepsilon}}^p = \sqrt{\frac{2}{3}\dot{\mathbf{H}}^p : \dot{\mathbf{H}}^p} \tag{31}$$

From figures 13(a) and (b), it can be seen that, at the onset of plastic deformation, plasticity starts in the same grains and at the same locations in 100-μm grains as in 1-μm grains. This is due to the fact that the same critical resolved shear stress is adopted for both grain sizes, that is, the same initial dislocation densities are assumed in both cases. In contrast, at higher mean plastic strain levels, the strongly different values of the plastic micro-deformation gradients lead to significantly different plastic strain fields. Two main features are evidenced in figure 13(c) to (f). Firstly, a tendency to strain localization in bands is observed for small grain sizes. The strain localization bands cross several grains, whereas plastic strain becomes more diffuse at larger grain sizes, which is something that had already been seen in the simulations presented in [24]. Secondly, a consequence of this localization is that some small grains are significantly less deformed than the larger ones. These features are also visible on the plastic deformation maps of figure 13 for the same aggregate but different grain sizes. This figure also shows the field of the dislocation density tensor norm:

$$\left\|\boldsymbol{\Gamma}_{\chi}\right\| := \sqrt{\boldsymbol{\Gamma}_{\chi} : \boldsymbol{\Gamma}_{\chi}} \tag{32}$$

This scalar quantity indicates the presence of GNDs and has the physical dimension of lattice curvature (mm−1). In large grains, GNDs are mainly located close to grain boundaries. At smaller grain sizes, the GND densities become significantly greater and spread over larger zones within the grains. Note also that pile-up like structures close to grain boundaries are clearly visible in the 10-μm grain aggregate. It should be noted that strain gradient plasticity models may be prone to strain localization when plasticity is confined to small regions. The reason for such behavior is that intense slip bands that exhibit a strong gradient of plastic slip perpendicular to the slip plane are not associated with GND formation. In contrast, regions of high lattice curvature or kink bands lead to an energy increase. This explains why, at small scales, intense slip bands are preferred to strongly curved regions and pile-ups.

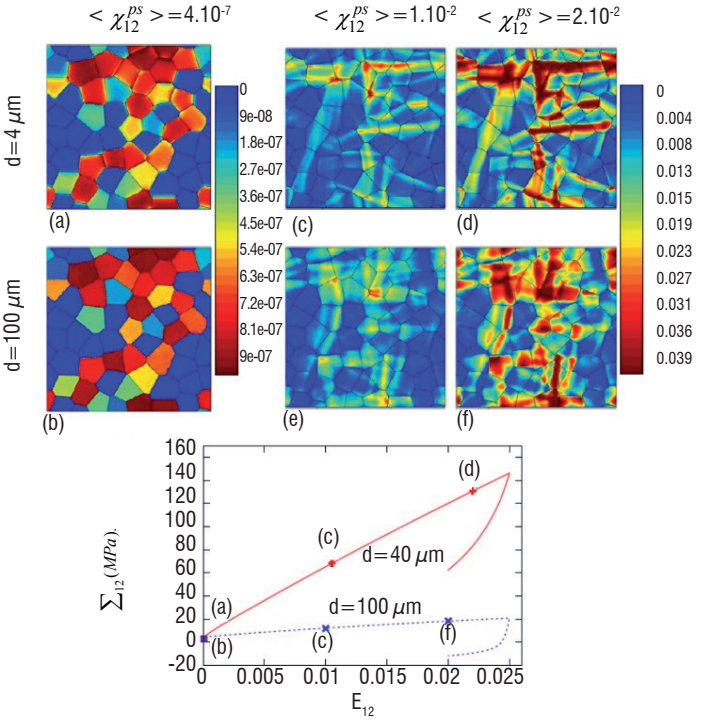

Figure 13 - (a)–(f) Contour plots of the accumulated plastic strain $\tilde{\varepsilon}^p$ for two grain sizes, d = 100 and 4 μm, and different mean values of the plastic strain: $\chi_{12}^{ps} \approx 0.0$, 0.01 and 0.02, obtained with a 2D 55-grain aggregate under simple shear, (g) macroscopic stress–strain response of the corresponding aggregate, with the letters indicating the different loading steps corresponding to the (a)–(f) contour plots [23]

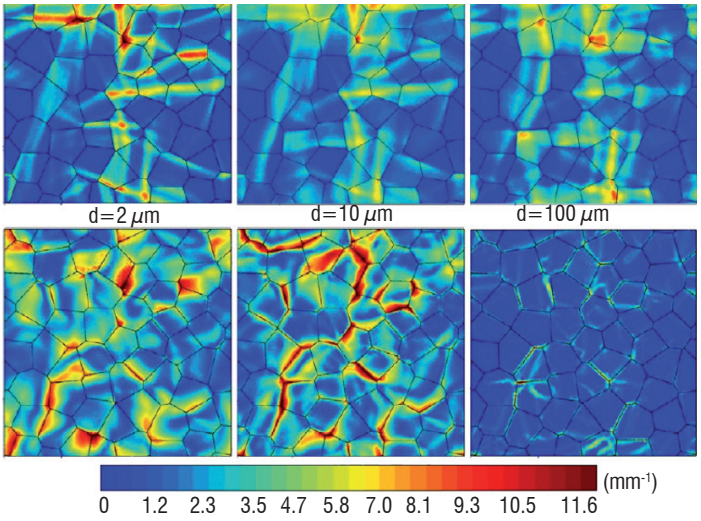

Figure 14 - Grain size effect on the accumulated plastic strain, (top figures), and on the norm of the dislocation density tensor, (bottom figures). These contour plots are obtained with the 2D 55-grain aggregate for the same mean value of $\chi_{12}^{ps} = 0.01$. The color scale for the plastic strain field of the top figures is the same as that of figure 12 on the right. The color scale at the bottom is that for the dislocation density tensor fields [23]

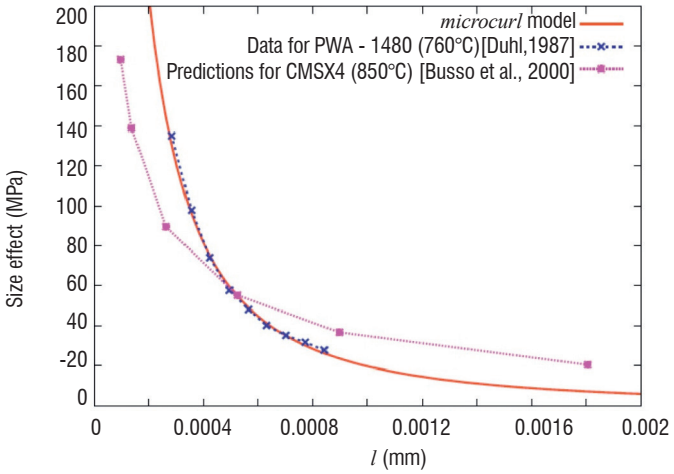

Figure 15 - Comparison between experimental data, in the form of precipitate size vs. size effect strengthening from a two-phase material (elasto-viscoplastic γ phase matrix with an embedded 68% quasi-elastic γ' precipitates) from Duhl (1987), the prediction of [16] and that obtained using the *microcurl* model [25]

In summary, the microcurl model was found to naturally predict a size-dependent kinematic hardening behavior, which is responsible for the observed strong size effects. Furthermore, the study showed that the flow stress attained at a given averaged plastic strain follows a power law scaling relation with the grain size, for grain sizes larger than a critical value. Likewise, the predicted plastic deformation fields were found to be strongly affected by grain size, with micron-size grain regions exhibiting the formation of intense slip bands crossing several grains. Finally, the dislocation density tensor, $\boldsymbol{\Gamma}_{\chi}$, was found to impact not only the overall polycrystal behavior, but also to control the way in which plastic deformation develops within the grains.

In Cordero et al. [23], it was shown that the microcurl approach could also be successfully used to predict experimentally observed precipitate size effects in two-phase single crystal nickel based superalloys. This is shown in figure 15, where a comparison between experimental data, in the form of precipitate size vs. size effect strengthening from a two-phase superalloy material (γ phase matrix with an embedded 68% γ' precipitates), the predictions of Busso et al. [16] and that obtained using the microcurl model [25] are shown. It can be seen that the microcurl model is able to simulate a precipitate size effect naturally. Moreover, the identified characteristic length, $lc=200\ nm$, is approximately the matrix channels width in Ni-base superalloys.

Concluding remarks

The various constitutive modeling approaches that address a broad range of phenomena at either the single crystal or the polycrystalline levels have been discussed. This overview has also highlighted the rich variety of physical, computational and technological issues within the broad area of micromechanics, which have been successfully addressed, and has identified some theoretical and computational difficulties and challenges for future developments. Recent advances in measuring and observation techniques, such as 2D and 3D image correlation, tomography, high resolution EBSD, in-situ TEM and SEM testing, combined spectroscopy and SEM, computational power and parallel processing are opening great new opportunities for the validation and implementation of predictive crystal plasticity based models. In this overview, it has been shown that size effects can be captured realistically by the curl of the plastic strain, or dislocation density tensor; however a better accounting of physical properties via cross-graining (multi-scale links) is needed. In future research, statistical effects will also need to be considered more thoroughly. The effects of grain dislocation substructures are also still too phenomenological. Crystal plasticity is also increasingly relied upon to study grain boundary - dislocation interaction (e.g., pile-ups) phenomena. Moreover, the coupling of crystal plasticity with phase field approaches to study grain complex phenomena, such as grain boundary / inter-face migration or phase transformation has now became a reality. However, even though it is still computationally too expensive, its potential is huge. Finally, the coupling of multi-physics approaches with crystal plasticity to account for time-dependent processes (e.g., dislocation climb, point-defect diffusion, irradiation damage) has recently been shown to be a logical and promising evolution and to open up exciting new opportunities to study complex coupled phenomena ■

Acknowledgements

The author would like to acknowledge the contributions of his PhD students and Post-Doctoral researchers to this work over the years, in particular F. Meissonnier, K. Cheong, G. Abrivard, N. Cordero, and his colleagues S. Forest (Ecole des Mines de Paris) and N. ODowd (University of Limerick). The support received from Siemens-UK, Hitachi-Japan, the European Commission (through the project DIGIMAT, contract number NMP3-CT-2006-017105), the UK's EPSRC and France's ANR to study single crystal behavior is greatly appreciated

References

[1] G. ABRIVARD - *A Coupled Crystal Plasticity - Phase Field Formulation to Describe Microstructural Evolution in Polycrystalline Aggregates during Recrystallisation*. Doctoral Thesis, Centre des Matériaux, Ecole des Mines de Paris, France (2009).
[2] G. ABRIVARD , E.P. BUSSO, S. FOREST, B. APPOLAIRE - *Phase Field Modelling of Grain Boundary Motion Driven by Curvature and Stored Energy Gradient*. Part I – Theory and Numerical Implementation, Philo-sophical Magazine, V. 92, Issue 28-30: 3618-3642 (2012a).
[3] G. ABRIVARD, E.P. BUSSO, S. FOREST, B. APPOLAIRE - *Phase Field Modelling of Grain Boundary Motion Driv-en by Curvature and Stored Energy Gradient.* Part II – Application to Thermal Recrystalisation", Philo-sophical Magazine, V. 92, Issue 28-30: 3643-3664 (2012b).
[4] A. ACHARYA, J.L. BASSANI - *Lattice Incompatibility and a Gradient Theory of Crystal Plasticity.* Journal of the Mechanics and Physics of Solids 48: 1565–1595 (2000).
[5] A. ACHARYA, A.J. BEAUDOIN - *Grain Size Effects in Viscoplastic Polycrystals at Moderate Strains*. Journal of the Mechanics and Physics of Solids 48: 2213–2230 (2000).
[6] E.C. AIFANTIS - *On the Microstructural oOrigin of Certain Inelastic Models*. Journal of Engineering Mate-rials and Technology 106: 326–330 (1984).
[7] E.C. AIFANTIS - *The Physics of Plastic Deformation*. International Journal of Plasticity 3: 211–248 (1987).

[8] L. ANAND, M .KOTHARI - *A Computational Procedure for Rateindependent Crystal Plasticity*. J. Mech. Phys. Solids 44: 525-558 (1996).
[9] A. ARSENLIS, D. PARKS - *Modeling the Evolution of Crystallographic Dislocation Density in Crystal Plasticity*. J. Mech. Phys. Solids 50: 1979-2009 (2001).
[10] R.J. ASARO, J.R. RICE - *Strain Localization in Ductile Single Crystals*. J. Mech. Phys. Solids 25: 309-338 (1977).
[11] D.J. BAMMANN - *A Model of Crystal Plasticity Containing a Natural Length Scale*. Materials Science and Engineering A 309–310: 406–410 (2001).
[12] J.L. BASSANI - *Incompatibility and a Simple Gradient Theory of Plasticity*. Journal of the Mechanics and Physics of Solids 49: 1983–1996 (2001).
[13] E. BITTENCOURT, A. NEEDLEMAN, M. GURTIN, E .VAN DER GIESSEN - *A Comparison of Nonlocal Continuum and Discrete Dislocation Plasticity Predictions.* Journal of the Mechanics and Physics of Solids 51 (2): 281–310 (2003).
[14] E.P. BUSSO - PhD Thesis, Department of Mechanical Engineering, Massachusetts Institute of Technology, Cambridge, MA,USA (1990).
[15] EP. BUSSO, F. MCCLINTOCK - *A Dislocation Mechanics-Based Crystallographic Model of a B2-Type Intermetallic Alloy*. Int. J. Plasticity 12: 1-28 (1996).
[16] E.P. BUSSO, F.T.MEISSONNIER, N.P. O'DOWD - *Gradient-Dependent Deformation of Two-Phase Single Crystals*. J. Mech. Phys. Solids 48: 2333-2361 (2000).
[17] E.P. BUSSO, G.CAILLETAUD - On the Selection of Active Slip Systems in Crystal Plasticity. Int. J. Plasticity, 21: 2212–2231 (2005).
[18] E.P. BUSSO - Chapter on *"From Single Crystal to Polycrystal Plasticity: An Overview of Main Ap-proaches".* "Handbook of Damage Mechanics: Nano to Macro Scale for Materials and Structures", George Z. Voyiadjis (ed.), Spinger (publ.), 369-394 (2014).
[19] K.S. CHEONG, E.P. BUSSO - *Discrete Dislocation Density Modelling of Single Phase FCC Polycrystal Aggregates*. Acta Materialia 52: 5665–5675 (2004).
[20] K.S. CHEONG, E.P. BUSSO, A. ARSENLIS - *A Study of Microstructural Length Scale Effects on the Behavior of FCC Polycrystals Using Strain Gradient Concepts.* International Journal of Plasticity 21: 1797–1814 (2004).
[21] K.S. CHEONG, E.P. BUSSO - *Effects of Lattice Misorientations on Strain Heterogeneities in FCC Polycrystals*. Journal of the Mechanics and Physics of Solids 54 (4): 671–689 (2006).
[22] J.D. CLAYTON, D.L. MCDOWELL, D.J. BAMMANN - *Modeling Dislocations and Disclinations With Finite Mi-Cropolar Elastoplasticity*. International Journal of Plasticity 22: 210–256 (2006).
[23] N.M. CORDERO, A. GAUBERT, S. FOREST, E.P. BUSSO F. GALLERNEAU, S. KRUCH - *Size Effects in General-Ised Continuum Crystal Plasticity for Two-Phase Laminates*. Journal of the Mechanics and Physics of Solids, 58 : 1963–1994 (2010).
[24] N.M. CORDERO, S. FOREST, E.P. BUSSO, S. BERBENNI, M. CHERKAOUI - *Grain Size Effects on Plastic Strain and Dislocation Density Tensor Fields in Metal Polycrystals*. Computational Materials Science, 52 : 7-13 (2012a).
[25] N.M. Cordero, Forest S, E.P. BUSSO - *Generalised Continuum Modelling of Grain Size Effects in Polycrystals*. Comptes Rendus Mécanique, 340 : 261-264 (2012b).
[26] M.A. CRISFIELD - *Non-linear Finite Element Analysis of Solids and Structures*. Vol. 1 & 2, 4th edn, John Wiley & sons, New York (1997).
[27] F. DELAIRE, J.L. RAPHANEL, C. REY - *Plastic Heterogeneities of a Copper Multicrystal Deformed in Uniaxial Tension: Experimental Study and Finite Element Simulations.* Acta Mater; 48: 1075–87 (2000).
[28] F.P.E. DUNNE, R. KIWANUKA, A.J.WILKINSON - *Crystal Plasticity Analysis of Micro-Deformation, Lattice Rotation and Geometrically Necessary Dislocation Density*. Proc. Royal Society A-Math. Phys. And Eng. Sciences, Vol 468: 2509-2531 (2012).
[29] F.P.E. DUNNE, D. RUGG, A. WALKER - *Length Scale-Dependent, Elastically Anisotropic, Physically-Based HCP Crystal Plasticity: Application to Cold-Dwell Fatigue in Ti Alloys*. Int. J. of Plasticity, Vol 23: 1061-1083 (2007).
[30] D.N. DUHL - *Directionally Solidified Superalloys.* Superalloys II - High Temperature Materials for Aerospace and Industrial Power. Wiley-Interscience, John Wiley and Sons, pp. 189–214 (1987).
[31]A.C. ERINGEN, W.D. CLAUS - *A Micromorphic Approach to Dislocation Theory and its Relation to Several Existing Theories*. Simmons, J.A., de Wit, R., Bullough, R. (Eds.), Fundamental Aspects of Dislocation Theory. National Bureau of Standards (US) Special Publication 317, II,: 1023–1062 (1970).
[32] N.A. FLECK, J.W. - HUTCHINSON - *Strain gradient plasticity*. Advances in Applied Mechanics 33: 295–361 (1997).
[33] S. FOREST, F. PRADEL, K. SAB - *Asymptotic analysis of heterogeneous Cosserat media*. International Journal of Solids and Structures 38: 4585–4608 (2001).
[34] S. FOREST, R. SEDLACEK - *Plastic Slip Distribution in Two-Phase Laminate Microstructures: Dislocation-Based VS. Generalized-Continuum Approaches*. Philosophical Magazine A 83: 245–276 (2003).
[35] N.M. GHONIEM, E.P. BUSSO, H. HUANG, N. KIOUSSIS - *Multiscale Modelling of Nanomechanics and Micromechanics: an Overview*. Philosophical Magazine, 83: 3475-3528 (2003).
[36] ME GURTIN - *A Gradient Theory of Single-Crystal Viscoplasticity that Accounts for Geometrically Necessary Dislocations*. Journal of the Mechanics and Physics of Solids 50: 5–32 (2002).
[37] M.E. GURTIN, L. ANAND - *Thermodynamics Applied to Gradient Theories Involving the Accumulated Plastic Strain: the Theories of Aifantis and Fleck & Hutchinson and Their Generalization*. Journal of the Mechanics and Physics of Solids 57: 405–421 (2009).
[38] S. KALIDINDI, C. BRONKHORST, L. ANAND - *Crystallographic Texture Theory in Bulk Deformation Processing of FCC Metals*. J. Mech. Phys. Solids 40: 537 (1992).
[39] T.M. HATEM, M.A. ZIKRY - *Dislocation Density Crystalline Plasticity Modeling of Lath Martensitic Microstructures in Steel Alloys.* Philosophical Magazine, 89(33): 3087-3109 (2009).
[40] R. HILL - *The Mathematical Theory of Plasticity*. 4th edn, Clarendon Press,Oxford, U.K. (1950).
[41] N. HUBER, C. TSAKMAKIS - *Determination of Constitutive Properties from Spherical Indentation Data Using Neural Networks*. *Part II: Plasticity with Nonlinear Isotropic and Kinematic Hardening*. J. Mech. Phys. Solids 47: 1589-1607 (1999).
[42] D. HUGHES - *Microstructure Evolution, Slip Patterns and Flow Stress*. Materials Science and Engineering A-Structural Materials Properties Microstructure and Processing, 319:46–54 (2001).
[43] A. HUNTER, M. KOSLOWSKI - *Direct Calculations of Material Parameters for Gradient Plasticity.* Journal of the Mechanics and Physics of Solids 56 (11): 3181–3190 (2008).
[44] U.F. KOCKS, C.N. TOME, H.R. WENK - *Texture and Anisotropy: Preferred Orientations in Polycrystals and their Effect on Material Properties.* Cambridge University Press, UK (2000).
[45] H. LIANG, F. P. E. DUNNE - *GND Accumulation in Bi-Crystal Deformation: Crystal Plasticity Analysis and Comparison With Experiments.* International Journal of Mechanical Sciences, 51(4):326–333 (2009).
[46] Q. LIU, D. JENSEN, N. HANSEN - *Effect of Grain Orientation on Deformation Structure in Cold-Rolled Polycrystalline Aluminium.* Acta Materialia, 46(16):5819–5838 (1998).
[47] J. MANDEL - *Plasticité classique et viscoplasticité*. CISM Course N°. 97, Springer-Verlag, Wien(1972).
[48] D.L. MCDOWELL - Materials Cience and Engineering Reports; 62(3°: 67-123 (2008).
[49] F. MEISSONNIER, E.P. BUSSO, N.P. O'DOWD - *Finite Element Implementation of a Generalised Non-Local Rate-Dependent Crystallographic Formulation for Finite Strains*. International Journal of Plasticity, V. 17, Issue 4: 601-640 (2001).

[50] C-W. Nan, D. Clarke - *The Influence of Particle Size and Particle Fracture on the Elastic-Plastic Deformation of Metal Matrix Composites.* Acta Mater. 44: 3801-3811 (1996).
[51] J.F. NYE - *Some Geometrical Relations in Dislocated Crystals*. Acta Metallurgica 1: 153–162 (1953).
[52] B. PEETERS, M. SEEFELDT, C. TEODOSIU, S.R. KALIDINDI, P. VANHOUTTE, E. AERNOUDT - *Work-Hardening/Softening Behaviour of B.C.C. Polycrystals Udring Changing Strain Paths: I. An integrated Model Based on Substructure and Texture Evolution, and its Prediction of the Stress–Strain Behaviour of an IF Steel During Two-Stage Strain Paths*. Acta Mater V 49:1607–19 (2001).
[53] E. POUILLIER, A.F. GOURGUES, D. TANGUY, E.P. BUSSO - *A Study of Intergranular Fracture in an Aluminium Alloy Due to Hydrogen Embrittlement.* International Journal of Plasticity, 34: 139-153 (2012).
[54] D. RAABE, Z. ZHAO, M. MAO - *On the Dependence of in-Grain Subdivision and Deformation Texture of Aluminum on Grain Interaction*. Acta Mater. 50: 4379–4394 (2002)..
[55] D. RAABE, M. SACHTLEBER, , H. WEILAND, G. SCHEELE, Z. ZHAO - *Grain-Scale Micromechanics of Polycrystal Surfaces During Plastic Straining*. Acta Mater. 51: 1539–1560 (2003).
[56] F. SCHUBERT, G. FLEURY, T. STEINHAUS - *Modelling of the Mechanical Behaviour of the SC Alloy CMSX-4 During Thermomechanical Loading*. Modelling Simul. Sci. Eng. 8: 947-957 (2000).
[57] J.Y. SHU - *Scale-Dependent Deformation of Porous Single Crystals*. International Journal of Plasticity 14: 1085–1107 (1998).
[58] P. Steinmann - *Views on Multiplicative Elastoplasticity and the Continuum Theory of Dislocations*. International Journal of Eng. Science 34: 1717–1735 (1996).
[59] B. SVENDSEN - *Continuum Thermodynamic Models for Crystal Plasticity Including the Effects of Geometrically-Necessary Dislocations.* Journal of the Mechanics and Physics of Solids 50: 1297–1329 (2002).
[60] J. SWADENER, A. MISRA, R. HOAGLAND, M. NASTASI - *A Mechanistic Description of Combined Hardening and Size Effects*. Scripta Met. 47: 343-348 (2002).
[61] A. TATSCHL, O. KOLEDNIK - *On the Experimental Characterization of Crystal Plasticity in Polycrystals*. Mater. Sci. Eng. A 342, 152–168 (2000).
[62] S. ZAEFFERER, J.C. KUO, Z. ZHAO, M. WINNING, D. RAABE - *On the Influence of the Grain Boundary Misorientation on the Plastic deformation of Aluminum Bicrystals*. Acta Mater: 51, 4719–4735 (2003).
[63] N. ZHANG, W. TONG - *An Experimental Study on Grain Deformation and Interactions in an Al–05% Mg Multicrystal*. Int. J. Plasticity 20: 523–542 (2004).
[64] M.A. ZIKRY, M. KAO - *Inelastic Microstructural Failure Mechanisms in Crystalline Materials With High Angle Grain Boundaries.* J Mech Phys Solids V 44(11):1765–98 (1996).

AUTHORS

Esteban P. Busso is currently the Scientific Director of ONERA's Materials and Structures Branch. He was formerly Professor of Mechanics of Materials at the Ecole des Mines de Paris and director of the Ecole's Centre des Matériaux and, from 1994 till 2005, Professor at Imperial College's Department of Mechanical Engineering in London, UK. He obtained his MSc and PhD degrees from the Massachusetts Institute of Technology (MIT) in Cambridge, USA, in 1987 and 1990, respectively. He also worked in industry in the UK, Japan, South Africa and Argentina. His research involves micromechanics studies of deformation and fracture of materials and interfaces, with an emphasis on the development of multiscale and multiphysics concepts in mechanistic models to predict deformation and fracture processes.